# Electron Paramagnetic Resonance Signals from the $S_3$ State of the Oxygen-Evolving Complex. A Broadened Radical Signal Induced by Low-Temperature Near-Infrared Light Illumination†

Nikolaos Ioannidis* and Vasili Petrouleas*

*Institute of Materials Science, NCSR "Democritos", 15310 Aghia Paraskevi, Attikis, Greece*

*Received January 20, 2000; Revised Manuscript Received March 9, 2000*

ABSTRACT: The tetranuclear manganese cluster responsible for the oxidation of water in photosystem II cycles through five redox states denoted $S_i$ ($i = 0, 1, 2, 3, 4$). Progress has been made recently in the detection of weak low-field EPR absorptions in both the perpendicular and parallel modes, associated with the integer spin state $S_3$ [Matsukawa, T., Mino, H., Yoneda, D., and Kawamori, A. (1999) *Biochemistry 38*, 4072−4077]. We confirm observation of these signals and have obtained them in high yield by illumination of photosystem II membranes, in which the non-heme iron was chemically preoxidized. It is shown that a split $g = 4$ signal accompanies the $S_3$ state signals. The signals diminish in the presence of ethanol and vanish in the presence of methanol. This effect is similar to that exerted by these alcohols to the high-spin component ($g = 4.1$) of the $S_2$ state and suggests that the latter spin configuration is the precursor of the $S_3$ state low-field signals. The $S_3$ state shows similar sensitivity to infrared illumination as has been observed previously in the $S_2$ state [Boussac, A., Un, S., Horner, O., and Rutherford, A. W. (1998) *Biochemistry 37*, 4001−4007]. Illumination of the $S_3$ state with near-infrared light (700−900 nm), at temperatures around 50 K, results in the modification of the low-field signals and most notably to the appearance of a broad ($\Delta H \sim 200$ G) radical-type signal centered at $g = 2$. The signal is tentatively assigned to the interaction of the Mn cluster in a modified $S_2$ state with a radical.

The water splitting process is catalyzed by photosystem II (PSII)[1] periodically during a sequence of light-driven charge separation events. The main parts of the electron transport chain are the electron donor side, the light-sensitive chlorophyll species $P_{680}$, and the electron acceptor side (see ref *1* for a general review). $P_{680}$ is the primary site of the light excitation to charge separation conversion. The electron is transferred to the acceptor side and the hole to the donor side. The terminal electron acceptor is a $(quinone)_A$−iron-(II)−$(quinone)_B$ complex (see ref *2* for a review). Plastoquinone $Q_A$ is a single electron acceptor while plastoquinone $Q_B$ is a binary electron acceptor. The non-heme iron, if chemically oxidized, acts as an additional electron acceptor (reviewed in ref *3*). The donor side oxidizes two molecules of water for every four consecutive charge separation events. Key elements of the water-oxidizing complex (WOC) [equivalently, oxygen-evolving complex (OEC)] are a tetranuclear Mn cluster with its $Ca^{2+}$ and $Cl^-$ cofactors, and $Y_z$, which acts as a fast electron donor intermediate between the Mn cluster and $P_{680}^+$ (see refs *4*−*8* for general reviews). According to recent perceptions $Y_z$ has a more direct involvement in water oxidation, acting as an $e^-/H^+$ (*7*, *9*) or hydrogen atom abstractor (*10*, *11*) (but see alternative views reviewed in ref *12*). The OEC undergoes four one-electron oxidation state transitions, $S_0-S_1$, ..., $S_3-S_4$. $O_2$ is released during the $S_4-S_0$ transition. After prolonged dark adaptation the complex is found in the $S_1$ state.

Distinct Mn-centered EPR signals have been detected for the three lower S states. The $S_2$ state is characterized by half-integer spin signals: the extensively studied $S = 1/2$ multiline signal at $g = 2$ (*13*) and an alternative $S \geq 3/2$ signal at $g = 4.1$ (*14*, *15*). The size of the $g = 4$ signal, always present in a fraction of centers in untreated preparations, can be reduced by the addition of certain alcohols (few percent v/v) (*16*), most prominently by 5% v/v methanol (*17*), without alteration of the oxygen-evolving activity. The $S = 1/2$ multiline signal can be reversibly converted to the $g = 4.1$ signal via an intermediate $S \geq 5/2$ state ($g = 10$ and 6) by near-IR illumination at temperatures >60 K (*18*−*20*). Presumably, slightly differing Mn−ligand conformations are responsible for the stabilization of different spin ground states. The $S_1$ state is characterized by a weak integer spin EPR signal at $g = 4.8$ (*21*, *22*) and more recently by an alternative multiline signal at $g = 12$. The latter signal is detected in *Synechocystis* preparations but also, after removal of the 23 and 17 kDa extrinsic proteins, in spinach preparations (*23*). A half-integer spin signal has been detected more recently in the $S_0$ state produced either by chemical reduction (*24*) or after the 3rd

† This work was supported in part by EC Grant ERBFMRX-CT980214.

* Corresponding authors. N.I.: tel +301 650-3312; fax +301 6519430; e-mail nioannid@ims.demokritos.gr. V.P.: tel +301 650-3344; fax +301 6519430; e-mail vpetr@ims.demokritos.gr.

[1] Abbreviations: PSII, photosystem II; OEC, oxygen-evolving complex; WOC, water-oxidizing complex; BBY membranes, thylakoid membrane fragments enriched in PSII; S states, $S_0-S_4$ oxidation states of the water-oxidizing complex; Tyr Z or $Y_z$ and Tyr D or $Y_d$, the fast and slow tyrosine electron donors of PSII; signal II, the EPR spectrum of either of the two tyrosines; $Q_A$ and $Q_B$, the primary and secondary plastoquinone electron acceptors of PSII; cw EPR, continuous wave electron paramagnetic resonance; MES, 2-(*N*-morpholino)ethanesulfonic acid; chl, chlorophyll; EtOH, ethanol; MeOH, methanol.

10.1021/bi000131c CCC: $19.00 
Published on Web 04/15/2000

flash in a flash sequence (*25*, *26*). The presence of 0.5−3% v/v methanol is required for the observation of the weak hyperfine structure of the signal.

The observation of Mn-centered half-integer/integer/half-integer spin signals for the three states $S_0/S_1/S_2$ is consistent with the XANES data, indicating Mn oxidation during the one-electron $S_0-S_1$ and $S_1-S_2$ transitions (reviewed in ref *8*). There is less agreement concerning the nature of the $S_2-S_3$ transition. The majority of authors support the formation of a radical in the vicinity of the Mn cluster (*8*, *12*, *27*, *28*), but direct oxidation of the Mn during the $S_2$ to $S_3$ transition is favored by some authors (*29*, *30*). Indirect support to the former alternative is provided by recent fluorescence experiments indicating an unusually fast reduction of the $S_3$ state to $S_1$ by NO, compared with a 5 times slower reduction of $S_2$ to $S_1$ under similar conditions or with the slow reactivity of $S_3$ with other reductants (*31*). Chemical treatments that inactivate the OEC at the level of the $S_3$ state, $Ca^{2+}$ (*32*) or $Cl^-$ depletion and $NH_4Cl$ or acetate treatment (*33*−*38*), yield a modified $S_3$ state characterized by a 90−230 G broad $g = 2$ signal. The signal is attributed to a $S_2Y_z^{\bullet}$ state (*9*, *39*), which is unable to advance further. Theoretical simulations have been used to estimate the distance between $Y_z$ and the Mn cluster (*40*−*42*). The accuracy, however, of geometric distance determinations, when both exchange and dipolar couplings are present, has been questioned, and furthermore, important differences among the $S_2Y_z^{\bullet}$ signals have been noted at high frequencies (*43*). It is generally agreed, however, that $Y_z$ must be in close proximity to the Mn cluster, possibly close enough to participate in $H^+$/H transfer reactions (*7*, *9*−*11*). Until very recently no signals had been reported for the normal $S_3$ state.

A significant recent advance is the report of EPR signals associated with the $S_3$ state (*44*). These are low-field EPR signals with contributions in both the perpendicular and parallel mode at $g = 6.7-12$. Matsukawa et al. have attributed the signals to an $S = 1$ spin state. This state could result from the oxidation of the Mn cluster during the $S_2$ to $S_3$ transition or from a strong exchange coupling of an $S_2$ $S = {}^3/_2$ conformation with a radical (*44*). The $S_3$ signals are weak, and this, coupled with the difficulty in trapping the $S_3$ state in high yield, explains the belated detection of the signals.

In the present study a method is described, combining non-heme iron oxidation and continuous illumination under freezing in the presence of the $Q_B$ site inhibitor, atrazine, for the observation of the $S_3$ signals in high yield. The elimination of baseline artifacts allows the better characterization of the signal components. The effects of ethanol and methanol on the $S_3$ signals are related to the formation of the $S_3$ signal at the expense of the $S_2$ signals. Finally, it is shown that the $S_3$ state shows similar sensitivity to infrared illumination with the $S_2$ state (*19*). New signals are trapped at the expense of the old ones by infrared illumination at 50 K. Notable is the formation of a broadened radical signal at $g = 2$.

## MATERIALS AND METHODS

PSII-enriched thylakoid membranes were isolated from market spinach by standard procedures (*45*, *46*) with some modifications. Samples for EPR measurements were suspended in 0.4 M sucrose, 15 mM NaCl, and 40 mM MES, pH 6.5, at 6−8 mg of chl/mL and stored in liquid nitrogen until use. All samples in the present study contained approximately 0.5% v/v DMSO originating from the stock solution of atrazine (see below). Ethanol or methanol was added only in the experiments of Figures 2−4 as indicated in the figure legends.

The protocol for the $S_3$ state trapping was as follows. Samples were diluted to 1 mg of chl/mL and incubated with 2 mM $K_3Fe(CN)_6$ for 30 min at 4 °C to oxidize the non-heme iron. Ferricyanide was subsequently diluted to sub-micromolar levels by three consecutive wash steps in ferricyanide-free buffer. The pellet of the last centrifugation (the equivalent of several EPR samples in a set of experiments) was diluted in ferricyanide-free buffer containing 0.2 mM atrazine to a concentration of 6−8 mg of chl/mL for EPR studies. All the above steps were done in absolute darkness. Illumination was done with a 340 W projector lamp filtered (unless specifically mentioned otherwise) with a solution of $CuSO_4$ (absorption max around 800 nm) to diminish infrared light. Illuminations at 200 K (−70 to −80 °C) and −30 °C were for 4 min. Rapid freezing under illumination was carried by insertion of the EPR samples (initially in darkness at 4 °C) to a −80 °C bath under continuous illumination. Such illuminations were performed without the $CuSO_4$ solution filter in order to increase the light intensity and, as evidenced in Figure 1 (see below), are equivalent to illuminations performed at −30 °C with the filter present. Illumination at temperatures below 200 K was done inside the cavity with a water (absorbs above 900 nm) or water and a 3 mm RG715 SCHOTT filter (absorbs below 715 nm) or the $CuSO_4$ solution filter for a total of 1 min intermittently in 15 s intervals, to avoid heating of the sample. Following production of the $S_3$ state and possible additional illuminations at low temperatures, the samples were dark adapted for typically 60 min at 4 °C to return to the $S_1$ state. The resulting EPR spectrum was used as a reference and was subtracted from all other spectra to eliminate background contributions due to oxidized cyt $b_{559}$ and impurities. Following the dark adaptation the sample was illuminated again at −30 °C or −70 to −80 °C to obtain the maximum $S_2$ state population. The resulting states during the sequential treatments are summarized as follows:

$$S_1(\text{cyt } b_{559}^+)\cdots Q_A\text{Fe(III)} \xrightarrow{h\nu,\ 0 \text{ to } -80\ ^\circ\text{C}} S_3(\text{cyt } b_{559}^+)\cdots Q_A^-\text{Fe(II)}\cdots \xrightarrow{\text{dark, } 4\ ^\circ\text{C}}$$
$$S_1(\text{cyt } b_{559}^+)\cdots Q_A\text{Fe(II) (reference)} \xrightarrow{h\nu,\ -30 \text{ to } -80\ ^\circ\text{C}} S_2(\text{cyt } b_{559}^+)\cdots Q_A^-\text{Fe(II)}$$

EPR measurements were obtained with a Bruker ER-200D-SRC spectrometer interfaced to a personal computer and equipped with an Oxford ESR 900 cryostat, an Anritsu MF76A frequency counter, and a Bruker 035M NMR gaussmeter. Where not specified, the perpendicular 4102ST cavity was used, and the microwave frequency was 9.41 GHz with 4 mm tubes and 9.39 GHz with 5 mm tubes. The spectra obtained with the standard cavity are the average of two to four scans. Five mm tubes were exclusively used with the dual mode cavity, 4116 DM, and 4 or 10 accumulations were done in the perpendicular or the parallel mode, respectively.

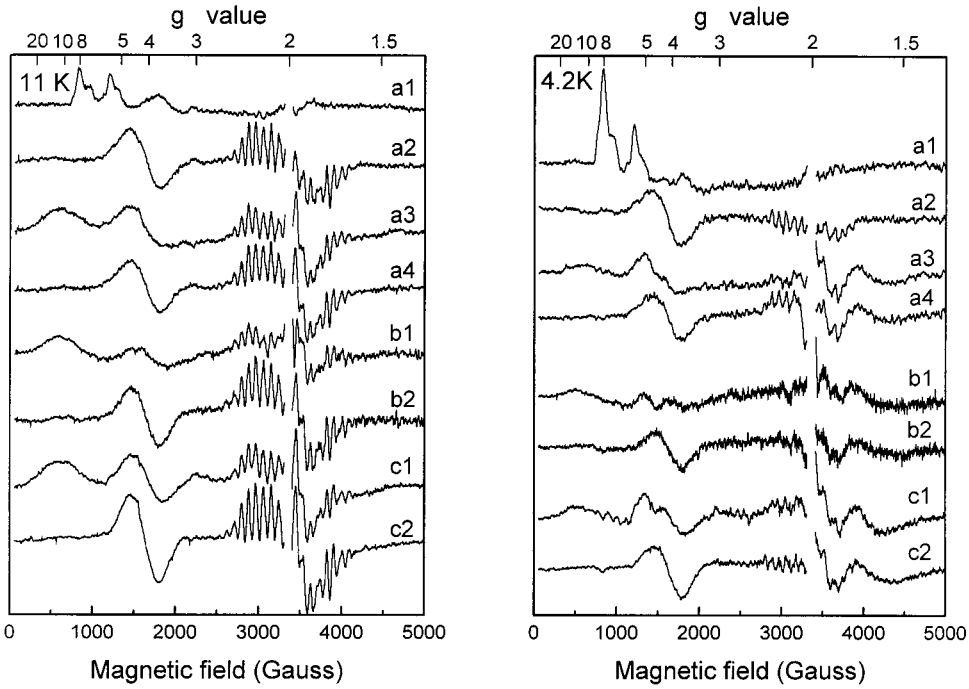


FIGURE 1: Trapping of the $S_3$ state by prior oxidation of the non-heme iron and illumination at different temperatures: (a1) following iron oxidation and addition of atrazine; (a2) illumination at 200 K resulting in formation of the $S_2\cdots Q_AFe(II)$ state; (a3) subsequent illumination at −30 °C resulting in reduction of $Q_A$ and formation of the $S_3$ state; (a4) dark adaptation for 60 min at 4 °C and subsequent illumination at 200 K to generate the $S_2\cdots Q_A^-Fe(II)$ state; (b1) similar sample as in (a) but illuminated directly at −30 °C; (b2) subsequent dark adaptation for 60 min at 4 °C and illumination at 200 K as in (a4); (c1) sample treated as in (a) but frozen under illumination (see Materials and Methods); (c2) subsequent dark adaptation for 60 min at 4 °C and illumination at 200 K as in (a4). All spectra are difference spectra obtained after subtraction of the dark-adapted spectrum recorded prior to the last illumination. EPR conditions: temperatures as indicated in the panels, microwave frequency 9.41 GHz, microwave power 38 mW, and modulation amplitude 25 G. The spectra at 4.2 K were scaled down by a factor of 1.4. Variation in the $S_2\cdots Q_A^-$ state signal intensity is due to varying chlorophyll concentrations among the different samples.

The microwave frequency was 9.60 GHz in the perpendicular mode and 9.31 GHz in the parallel mode. Oxygen, even at small concentrations, can distort severely the baseline in the studies employing the parallel mode. Accordingly, the samples were bubbled with pure nitrogen gas prior to these measurements.

## RESULTS AND DISCUSSION

*$S_3$ Perpendicular Mode Spectra.* Advancement of PSII from the dark stable state $S_1$ to $S_3$ requires two consecutive charge separations. This can be accomplished in a straightforward manner by pulsed-laser illumination. This limits, however, the EPR experiment to dilute samples, making the detection and characterization of the weak $S_3$ state signals difficult (*44*). Matsukawa et al. (*44*) have used continuous illumination (12 min) at 235 K to routinely observe the signal in concentrated samples. The observed decrease of the $S_2$ multiline signal attributed to advancement to a higher S state was relatively low, approximately 30%. Apparently this is due to the following limitations. The 235 K temperature is approximately the half-inhibition temperature for $S_2$ to $S_3$ and $S_3$ to $S_0$ advancements, as indicated by EPR (*47*, *48*) and thermoluminescence (reviewed in ref *49*) experiments. In addition, not all centers have the $Q_B$ site occupied, and occupation of the site after charge separation is kinetically limited at 235 K. Furthermore, a fraction of centers may advance beyond $S_3$ under these conditions. We have accordingly looked into improvements of the continuous illumination protocol. An approach that was proven efficient is the prior oxidation of the acceptor side non-heme iron and the blockage of the electron transfer to $Q_B$ by the use of inhibitors, e.g., atrazine. This leaves two potential one-electron acceptors, $Q_A$ and Fe(III). The temperature of illumination is an important factor to be considered. While the lower limit is set by the thermal barrier for the $S_2$ to $S_3$ advancement [the $S_1$ to $S_2$ transition has a much lower half-inhibition temperature of 135−140 K (*47*−*49*)], the upper limit is set by the stability of the charge separation, i.e., the recombination rate of $S_3$ with $Q_A^-$. The data on this recombination rate are rather scarce (*50*, *51*), but this rate should be similar to the $S_2-Q_A^-$ recombination rate. This is approximately 1 s at room temperature (*50*, *51*) and slows down to a $t_{1/2}$ of ca. 5 min at −25 °C (*52*, *53*). This latter rate has indeed been confirmed for the $S_3-Q_A^-$ recombination during our studies but will be examined in more detail in a future study.

Figure 1 compares EPR spectra of three similar samples prepared with the iron oxidized as described in Materials and Methods and following different illumination protocols. To enhance signal-to-noise ratio, the standard cavity has been used; therefore, only the perpendicular mode component of $S_3$ is observed. Prior to illumination the only contributions to the spectrum [Figure 1 (a1)] are from the acceptor side non-heme Fe(III) (*3*). Following illumination at 200 K the iron is reduced and the OEC advances to the $S_2$ state [Figure 1 (a2)] with the characteristic multiline signal at $g = 2$ and the alternative signal at $g = 4$. Subsequent illumination at −30 °C advances the OEC to the $S_3$ state [Figure 1 (a3)], as evidenced by the significant decrease of the $S_2$ multiline

signal and the appearance of a broad signal at low fields (500−600 G) similar to the signal attributed to the $S_3$ state by Matsukawa et al. (*44*). The new charge separation produces also the acceptor side $Q_A^-$Fe(II) signals in the 3500−4000 G region (*54*, *55*). Following prolonged dark adaptation at 4 °C the system relaxes to the $S_1$ state, as evidenced by the complete disappearance of all light-induced signals (spectrum not shown but used as a reference in obtaining the difference spectra). The system returns to the $S_2$ state by a new illumination at 200 K (or at any temperature between −30 and −80 °C). The spectrum [Figure 1 (a4)] shows $S_2$ signals equivalent in size with the spectrum in Figure 1 (a2), but in addition the $Q_A^-$Fe(II) signal is formed (see Materials and Methods). Qualitatively similar $S_3$ spectra (somewhat larger in size) are obtained if the initial illumination is at −30 °C [Figure 1 (b1)]. In this case the intermediate $S_2$ state cannot be trapped, but the full $S_2$ state is produced in Figure 1 (b2) following the dark adaptation and new illumination. Finally, illumination of a sample under freezing (see Materials and Methods) appears to produce consistently (in separate experiments not shown) somewhat larger $S_3$ signals [Figure 1 (c1)], with its respective $S_2$ spectrum obtained as shown above in Figure 1 (c2).

The $S_3$ signal in Figure 1 shows the general features reported by Matsukawa et al. (*44*) but appears to be better defined here. It is notable that the signal appears to be consistently accompanied by a split $g = 4$ signal more clearly apparent in the 4.2 K spectra [Figure 1 (b)]. This signal at 11 K is probably masked by the remaining $S_2$ state $g = 4$ signal. The low-field signal at about 500−600 G appears to be relatively weaker at 4.2 K, but this is due to partial saturation. A detailed study of the saturation properties of the signals as well as theoretical simulations will be published elsewhere. Another observation is that the $S_2$ signals are not fully eliminated under any illumination conditions. Judging from the decrease in the multiline signal, the efficiency of the trapping of the $S_3$ state ranges from 50% to 60%.

*Effect of Ethanol and Methanol on the $S_3$ Spectra.* Certain small alcohols enhance the $S_2$ multiline signal at the expense of the $g = 4$ signal although they do not inhibit advancement to the $S_3$ state or oxygen evolution (*16*). Notable examples are ethanol and particularly methanol (*16*, *17*). It has been reported by Matsukawa et al. (*44*) that the $S_3$ signal is not observed in the presence of methanol. We have examined the effects of ethanol and methanol on the $S_3$ and $S_2$ signals under our conditions. Figure 2 presents the $S_3$ (Figure 2a) and $S_2$ (Figure 2b) spectra, trapped in sequence as in Figure 1 (c1 and c2), in three identical samples differentiated by the absence or presence of the alcohols. The well-known progressive decrease of the $g = 4$ signal and the accompanying increase of the $S_2$ multiline signal are clearly observed in the spectra (Figure 2b). The $S_3$ signal at about 500−600 G (Figure 2a) shifts to higher field values, accompanied by an apparent decrease of its overall size in the presence of ethanol. No $S_3$ signal is discernible in the presence of methanol, in agreement with the observations of Matsukawa et al. (*44*). Despite differences in the $S_3$ signal size, all three samples show approximately the same fractional advancement to the $S_3$ state, as judged by the decrease in the $S_2$ multiline intensity by 50−60%. There are no new features in the spectra at 4.2 K, and these are not shown.

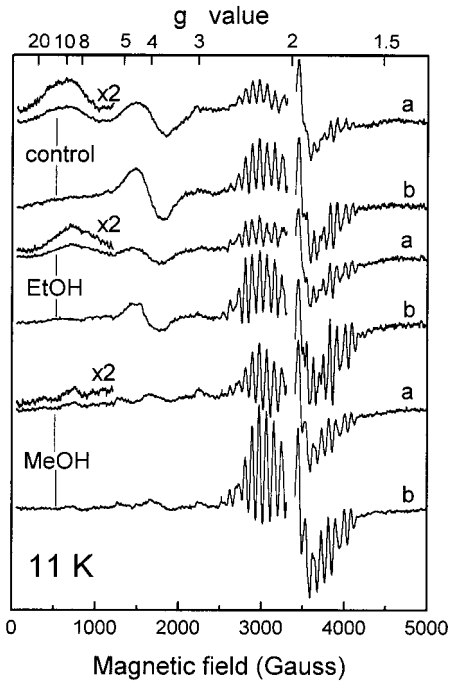


FIGURE 2: Comparison of $S_3$ (a) and $S_2$ (b) spectra produced as in Figure 1 (c1 and c2) in the absence (control) or presence of 5% v/v ethanol (EtOH) or 5% v/v methanol (MeOH). EPR conditions: $T = 11$ K; the rest as in Figure 1.

The effect of the alcohols is more clearly depicted in the parallel mode component of the $S_3$ spectrum. Figure 3 compares the respective spectra at 4 and 11 K. The spectra in the absence of alcohols (control) are similar to those reported by Matsukawa et al. (*44*). In the presence of ethanol the spectrum shifts to higher fields, and the intensity decreases significantly. No signal could be detected in the presence of methanol.

The spectra in Figures 2 and 3 show a correlation between the $S_2$ $g = 4$ signal intensity and the $S_3$ EPR signals, suggesting that only the $g = 4$ centers have an $S_3$ EPR signature under the present instrumental conditions. Whether this correlation is generally valid will have to be examined by future investigations. The possibility of heterogeneous multiline populations as described by Boussac (*56*) may also have to be considered.

*Comparison of the $S_3$ Signals with the High-Spin Signals of the $S_2$ State Induced by Infrared Light.* The $S_3$ signals in the perpendicular mode show a superficial similarity to the recently reported high-spin signals from the $S_2$ state. Boussac et al. (*19*) have shown that illumination at 65 K or lower with infrared light of samples poised to the $S_2 \cdots Q_A^-$Fe(II) state by previous white light illumination at 200 K produces low-field EPR signals at the expense of the $S_2$ multiline signal. We have confirmed that these signals can also be induced by the IR radiation present in the white light generated by our projector lamp (filtered only by water). As the high-spin signals appeared to be more readily inducible in the presence of ethanol [the published spectra by Boussac et al. (*19*) were also obtained in the presence of ethanol], we have compared the signals in the presence of this alcohol. Figure 4 compares the $S_3$ low-field spectra with the infrared light induced high-spin signal in the $S_2$ state. The $S_3$ and $S_2$ states were produced in the sequence as in Figure 1 (c1 and c2), but the $S_2$ state was further illuminated at 65 K. The

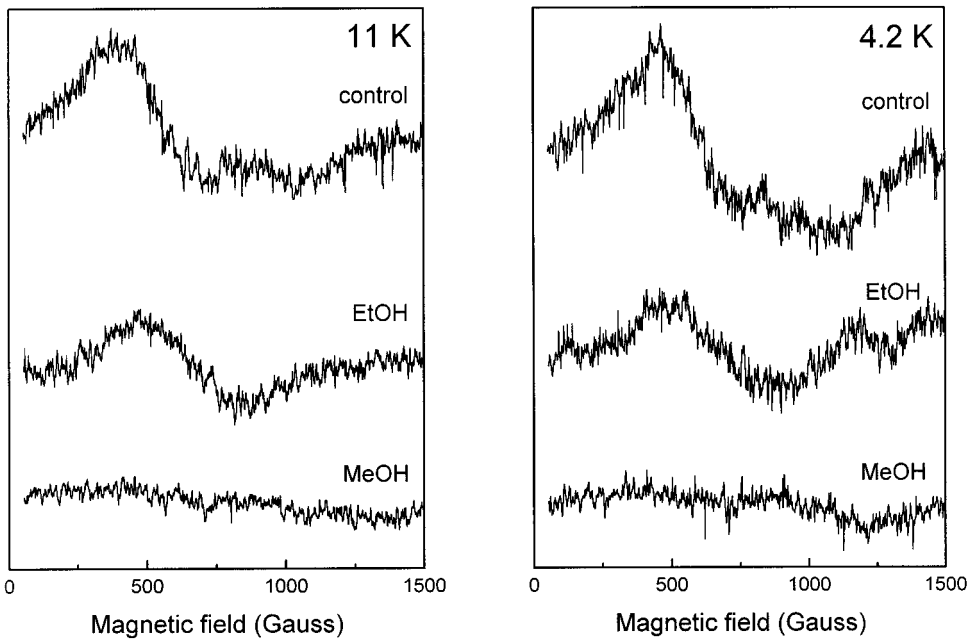


FIGURE 3: Parallel mode spectra of the $S_3$ state, trapped as in Figure 1 (c1), in the absence (control) or presence of 5% v/v ethanol (EtOH) or 5% v/v methanol (MeOH). EPR conditions: bimodal cavity, microwave frequency 9.31 GHz, microwave power 38 mW, and modulation amplitude 10 G.

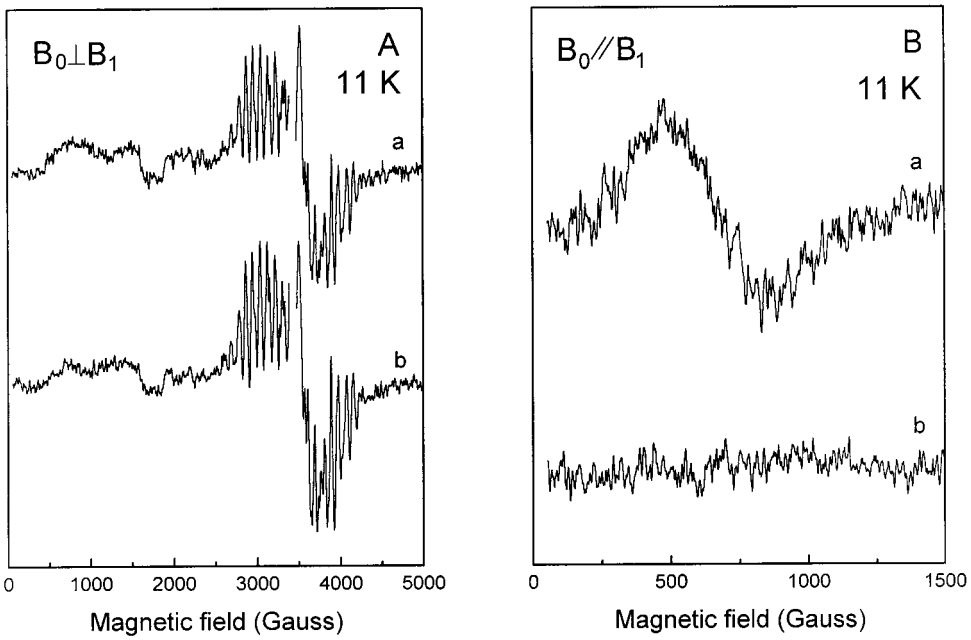


FIGURE 4: Comparison of the $S_3$ signals with the high-spin signals induced in the $S_2$ state by infrared light in the presence of 5% v/v ethanol. The $S_3$ (a) and $S_2$ states were produced in sequence as in Figure 1 (c1 and c2), but following $S_2$ formation the sample was illuminated at 65 K by white light filtered only with water (b). EPR conditions: bimodal cavity, microwave frequency 9.60 GHz in the perpendicular mode and 9.31 GHz in the parallel mode, microwave power 38 mW, and modulation amplitude 10 G. The spectra in the parallel mode have been scaled up by a factor of 10.

spectra are weak because the bimodal cavity was used in both modes for monitoring purposes. Given the lower modulation amplitude (10 vs 25 G with the standard cavity) and the lower quality factor, a lower signal-to-noise ratio by approximately a factor of 6 has been observed in comparison with the standard cavity for the broad signals. Nevertheless, low-field contributions can be observed in both spectra in the perpendicular mode. The signals appear in the same spectral region, but at this signal-to-noise ratio, it is difficult to examine differences. What is a clear difference is the absence of a parallel mode component in the infrared-excited $S_2$ state spectra. Experiments in the absence of ethanol have also confirmed the absence of a parallel mode component in the excited $S_2$ state spectra.

The absence of a parallel mode transition in the excited $S_2$ state spectrum is not surprising (although not strictly excluded in such a complex system) for half-integer spin. The general resemblance of the perpendicular mode spectra appears therefore fortuitous. The following interesting possibility will be, however, examined in future studies. The $S_3$ spectra result from a high-spin state of the Mn cluster, which is perturbed by a weak interaction with a radical.

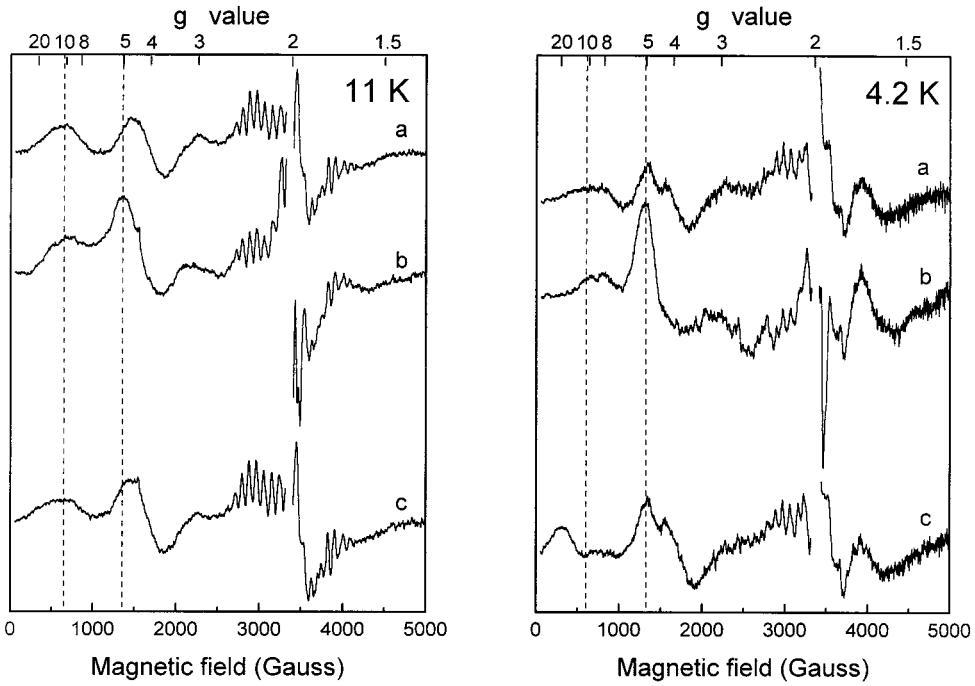


FIGURE 5: Effects of illumination at 50 K on the $S_3$ spectrum. (a) $S_3$ spectrum produced as in Figure 1 (c1). (b) Subsequent illumination at 50 K by unfiltered (water filter) light. (c) Annealing at 200 K for 2 min. EPR conditions: temperatures as indicated in the panels, microwave frequency 9.39 GHz, microwave power 38 mW, and modulation amplitude 25 G. The spectra at 4.2 K were scaled down by a factor of 1.2.

*Effects of Infrared Light Excitation on the $S_3$ State Signals: A Broad Radical Signal.* The effects of infrared light illumination on the $S_2$ signals (*19*) prompted us to examine likely effects on the $S_3$ state signals. Figure 5 compares the $S_3$ perpendicular mode spectra (a) prior or (b) following illumination at 50 K with water-filtered white light and (c) following subsequent annealing for 2 min at 200 K. Significant changes are observed following the illumination at 50 K in Figure 5b. A new signal appears in the $g = 2$ region. The signal is reminiscent of the broadened radical signal observed in the modified $S_3$ state (*32*−*43*) and will be examined in more detail below. The signal overlaps with the inner component of the $Q_A^-$Fe(II) signal, but it does not result from a modification of this state. Illumination at 50 K of samples in the $S_2 \cdots Q_A^-$Fe(II) state did not produce this signal. In addition to the $g = 2$ signal, pronounced signal intensity appears at $g = 5$, more clearly seen in the spectra at 4.2 K. The changes in the low-field $S_3$ signal are less clearly discerned in the spectra of Figure 5. The changes in this spectral region are also somewhat confused by the fact that part of the remaining $S_2$ multiline signal is converted to the high-spin form by the infrared illumination (*19*). This explains the small decrease in the multiline signal of Figure 5b. The parallel mode spectra shown in Figure 6 should not be affected by this effect, however (compare Figure 4B, trace b). An examination of Figure 5b and of the parallel mode spectra in Figure 6b suggests a 30−35% decrease in the low-field (at about 600 G) signal intensity and perhaps a slight shift to higher fields. Following 2 min annealing of the sample at 200 K, the $g = 2$ and $g = 5$ features disappear and the split $g = 4$ signal at 4.2 K is restored (Figure 5c). The signals at about 600 G appear shifted, however, to even lower fields in both the perpendicular (Figure 5c) and the parallel mode (Figure 6c) spectra. This latter change, which is more notable at 4.2 K, indicates a slightly different zero-field splitting of the spin levels. Higher annealing temperatures may be required for relaxation to the original configuration, but this could interfere with the decay of the $S_3$ state. A new illumination at 50 K following the annealing to 200 K induced the same signals as the first illumination. The effects of the low-temperature illumination are therefore reversible as has been noted with the $S_2$ state (*19*).

All signals induced by the 50 K illumination are significantly reduced (factor of 4) if the projector lamp is filtered with a $CuSO_4$ solution, which has an absorption maximum at about 800 nm. The signals, on the other hand, appear with undiminished intensity in the presence of a 3 mm SCHOTT RG 715 filter (absorbs below 715 nm) in addition to the water filter (absorbs above 900 nm). It is therefore concluded that near-infrared light is responsible for the observed spectral changes in the $S_3$ state, as has been observed with the $S_2$ state (*19*). The 50 K illumination experiments were repeated in the presence of ethanol or methanol. No significant changes were observed, and the broadened $g = 2$ signal could not be detected. The spectra in the presence of ethanol were also confused by the conversion of part of the remaining $S_2$ multiline signal to the high-spin form. This conversion appears to be more efficient in the presence of ethanol.

The broadened radical-type signal in Figure 5b is of significant interest and is examined in more detail in Figure 7. The spectra in Figure 7c,d were obtained by the subtraction of the $S_3$ state traces from the traces following illumination at 50 K (difference of traces b minus a in Figure 5). Spectrum b of Figure 7 has been similarly obtained but with 4 G modulation amplitude. Figure 7a is the spectrum (signal II) prior to the 50 K illumination and is included for reference. The apparent overall splitting of the broadened radical-type signal is approximately 200−230 G. The detailed structure of the inner part of the signal could not be clearly defined

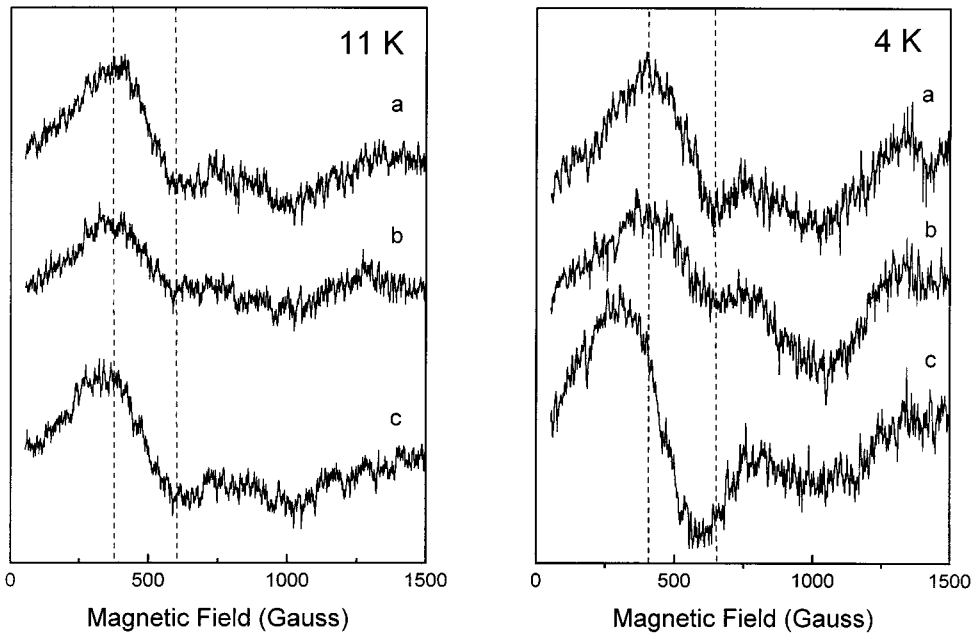


FIGURE 6: Effects of illumination at 50 K (water-filtered light) on the parallel mode $S_3$ state spectra. Spectral assignments as in Figure 5. The sample is different from the one in Figure 5, but the perpendicular mode spectra with the bimodal cavity (not shown) were similar to those in Figure 5. EPR conditions: bimodal cavity, microwave frequency 9.31 GHz, microwave power 38 mW, and modulation amplitude 10 G.

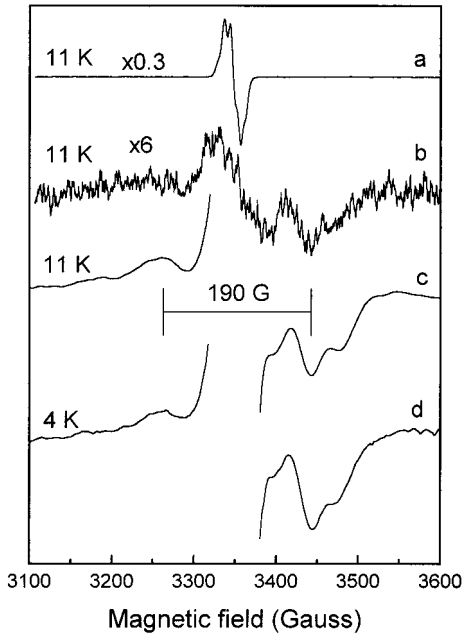


FIGURE 7: Expanded view of the $g = 2$ signal induced by the near-infrared light excitation of the $S_3$ state at 50 K. Difference spectra (b, c, and d) were obtained by subtraction of the respective $S_3$ spectra from the spectra obtained following subsequent illumination with water-filtered light at 50 K; spectrum a, given for reference, has been recorded under nonsaturating conditions prior to the 50 K illumination. EPR conditions: microwave frequency, 9.39 GHz; microwave power, (a) 0.057 mW, (b) 57 mW, and (c and d) 38 mW; modulation amplitude, (a and b) 4 G and (c and d) 25 G.

in spectra c and d due to the high modulation amplitude, which broadens the large background contribution from signal II. The spectrum in Figure 7b recorded with 4 G modulation amplitude indicates the presence of an inner component, the high-field part of which is also apparent as a shallow minimum at 3400 in the spectra c and d. The structure of the signal is reminiscent of the inhibited $S_3$ state signals (*32*−*43*). Integration of the spectrum in Figure 7b assuming that all signal intensity is contained within 3200 and 3550 indicated an area of 7−10% compared with signal II. This is not unreasonable if we assume that 50−60% of the $S_2$ centers advance to $S_3$ and of these presumably only a fraction (say 50%) is responsible for the low-field signals. The latter in turn are only partially excited (30−35%) by the infrared illumination.

The observation of a broadened radical signal induced by the infrared illumination may have important consequences in understanding the nature of the $S_3$ state. Although the action spectrum of the infrared light effect is not determined here, the window of 700−900 nm, set by the present experiments, closely matches the action spectrum of 820 nm ± 60 nm (half-width at half-maximum), reported for the induction of the low- to-high spin transition in the $S_2$ state (*18*, *19*). The latter is attributed to charge transfer within the cluster or a spin state change in a Mn(III) ion. More recently, Baxter et al. have correlated a NIR absorption band in the $S_2$ state with the NIR-induced spin transition (*57*). The absorption band is attributed to a spin-allowed d−d transition in a single Mn(III) ion. Apparently, the sensitivity to infrared illumination is preserved in the $S_3$ state. It would be premature at present to speculate on the structure of the $S_3$ state. Two general possibilities may be suggested, however: the $S_3$ state has a metalloradical character, and the NIR-induced spin transition/charge transfer within the cluster alters (weakens) the magnetic interaction of the cluster with the radical making the latter EPR visible. As, however, the magnetic interaction of the cluster with the radical is weak, we must assume that the radical is not one of the ligands to Mn but more remote. Alternatively, the infrared illumination excites the $S_3$ state (we do not address the nature of the $S_3$ here) to a potential high enough to oxidize a nearby residue (possibly $Y_z$), thus causing migration of the hole from the Mn cluster to the adjacent residue. In both alternatives, the signal at $g = 2$ is attributed to the interaction of a radical

(possibly $Y_z^{\bullet}$) with a modified $S_2$ state of the cluster. This appears to be similar to the situation encountered with the modified $S_3$ state (*32*−*43*) except that in the normal $S_3$ state the broadened radical signal results from an excited state of the complex.

## CONCLUSIONS

Two recent advances (*19*, *44*) motivated the present study. Matsukawa et al. (*44*) detected for the first time EPR signals attributed to the $S_3$ state. These are characterized by weak low-field EPR absorptions in both the parallel and the perpendicular mode. We confirmed the association of the signals with the $S_3$ state and optimized the conditions for their observation in high yield. The accurate baseline subtraction revealed a split $g = 4$ signal that appears to accompany the low-field signals at 500−600 G. The experiments in the presence of ethanol or methanol suggested a correlation between the low-field signals and the $g = 4$ $S_2$ state signal. Moreover, the unusual effect of infrared light excitation of the $S_2$ state, observed in the elegant studies of Boussac et al. (*19*), appears to have its counterpart in the $S_3$ state. Illumination by NIR (700−900 nm) light at 50 K induces significant changes in the signals that are difficult to interpret prior to a detailed theoretical analysis. One of the infrared light induced signals has, however, recognizable features of particular significance. This appears to be a broadened radical signal at $g = 2$ resembling the Tyr $Z^{\bullet}$ signal in the inhibited $S_3$ state (*32*−*43*). The latter signal is attributed to the magnetic interaction of the tyrosyl radical with the Mn cluster in the $S_2$ state. It is tentatively assumed that a similar state, $S_2^{*}\cdots R^{\bullet}$ (radical $R^{\bullet}$ could be $Y_z^{\bullet}$**),** is responsible for the radical signal in the infrared light excited $S_3$ state.

The up to very recently EPR-silent $S_3$ state appears now to be characterized by a variety of new signals that create hopes for advances in the elucidation of key steps in the catalytic mechanism of water oxidation.

## ACKNOWLEDGMENT

We thank Dr. Y. Sanakis, Dr. G. Schansker, and Ms. I. Sarrou for helpful discussions and Mr. P. Tampourlos for technical help. N.I. thanks I.K.Y. (Greek State Scholarship Foundation) for financial support.

## REFERENCES

1. Diner, B. A., and Babcock, G. T. (1996) in *Advances in Photosynthesis: Vol. 4. Oxygenic Photosynthesis: The Light Reactions* (Ort, R. D., and Yocum, C. F., Eds.) pp 213−247, Kluwer Academic Publishers, Dordrecht, The Netherlands.
2. Diner, B. A., Petrouleas, V., and Wendoloski, J. J. (1991) *Physiol. Plant. 81*, 423−436.
3. Diner, B. A., and Petrouleas, V. (1987) *Biochim. Biophys. Acta 895*, 107−125.
4. Rutherford, A. W. (1989) *Trends Biol. Sci. 14*, 227−232.
5. Debus, R. J. (1992) *Biochim. Biophys. Acta 1102*, 269−352.
6. Bricker, T. M., and Ghanotakis, D. F. (1996) in *Advances in Photosynthesis: Vol. 4. Oxygenic Photosynthesis: The Light Reactions* (Ort, R. D., and Yocum, C. F., Eds.) pp 113−136, Kluwer Academic Publishers, Dordrecht, The Netherlands.
7. Britt, R. D. (1996) in *Advances in Photosynthesis: Vol. 4. Oxygenic Photosynthesis: The Light Reactions* (Ort, R. D., and Yocum, C. F., Eds.) pp 137−164, Kluwer Academic Publishers, Dordrecht, The Netherlands.
8. Yachandra, V. K., Sauer, K., and Klein, M. P. (1996) *Chem. Rev. 96*, 2927−2950.
9. Gilchrist, M. L., Ball, J. A., Randall, D. W., and Britt, R. D. (1995) *Proc. Natl. Acad. Sci. U.S.A. 92*, 9545−9549.
10. Tommos, C., Tang, X.-S., Warncke, K., Hoganson, C. W., Styring, S., Mc-Cracken, J., Diner, B. A., and Babcock, G. T. (1995) *Photosynth. Res. 46*, 177−184.
11. Hoganson, C. W., and Babcock, G. T. (1997) *Science 277*, 1953−1956.
12. Haumann, M., and Junge, W. (1999) *Biochim. Biophys. Acta 1411*, 86−91.
13. Dismukes, G. C., and Siderer, Y. (1981) *Proc. Natl. Acad. Sci. U.S.A. 78*, 274−278.
14. Casey, J. L., and Sauer, K. (1984) *Biochim. Biophys. Acta 767*, 21−28.
15. Zimmermann, J. L., and Rutherford, A. W. (1984) *Biochim. Biophys. Acta 767*, 160−167.
16. Zimmermann, J. L., and Rutherford, A. W. (1986) *Biochemistry 25*, 4609−4615.
17. Pace, R. J., Smith, P., Bramley, R., and Stehlik, D. (1991) *Biochim. Biophys. Acta 1058*, 161−170.
18. Boussac, A., Girerd, J.-J., and Rutherford, A. W. (1996) *Biochemistry 35*, 6984−6989.
19. Boussac, A., Un, S., Horner, O., and Rutherford, A. W. (1998) *Biochemistry 37*, 4001−4007.
20. Horner, O., Riviere, E., Blondin, G., Un, S., Rutherford, A. W., Girerd, J.-J., and Boussac, A. (1998) *J. Am. Chem. Soc. 120*, 7924−7928.
21. Dexheimer, S. L., and Klein, M. P. (1992) *J. Am. Chem. Soc. 114*, 2821−2826.
22. Yamauchi, T., Mino, H., Matsukawa, T., Kawamori, A., and Ono, T. (1997) *Biochemistry 36*, 7520−7526.
23. Campbell, K. A., Gregor, W., Pham, D. P., Peloquin, J. M., Debus, R. J., and Britt, R. D. (1998) *Biochemistry 37*, 5039−5045.
24. Messinger, J., Nugent, J. H. A., and Evans, M. C. W. (1997) *Biochemistry 36*, 11055−11060.
25. Åhrling, K. A., Peterson, S., and Styring, S. (1997) *Biochemistry 36*, 13148−13152.
26. Messinger, J., Robblee, J. H., Yu, W. O., Sauer, K., Yachandra, V. K., and Klein, M. P. (1997) *J. Am. Chem. Soc. 119*, 11349−11350.
27. Styring, S. A., and Rutherford, A. W. (1988) *Biochemistry 27*, 4915−4923.
28. Siegbahn, P. E. M., and Crabtree, R. H. (1999) *J. Am. Chem. Soc. 121*, 117−127.
29. Ono, T., Nogushi, T., Inoue, Y., Kusunoki, M. T., Matsushita, T., and Oyanagi, H. (1992) *Science 258*, 1335−1337.
30. Iuzzolino, L., Dittmer, J., Doerner, W., Meyer-Klaucke, H., and Dau, H. (1998) *Biochemistry 37*, 17112−17119.
31. Ioannidis, N., Schansker, G., Barynin, V., and Petrouleas, V. (2000) *J. Biol. Inorg. Chem.* (in press).
32. Boussac, A., Zimmermann, J.-L., and Rutherford, A. W. (1989) *Biochemistry 28*, 8984−8989.
33. Sivaraja, M., Tso, J., and Dismukes, G. C. (1989) *Biochemistry 28*, 9459−9464.
34. Ono, T., and Inoue, Y. (1990) *Biochim. Biophys. Acta 1020*, 269−277.
35. Baumgarten, M., Philo, J. S., and Dismukes, G. C. (1990) *Biochemistry 29*, 10814−10822.
36. Andreasson, L.-E., and Lindberg, K. (1992) *Biochim. Biophys. Acta 1100*, 177−183.
37. MacLachlan, D. J., and Nugent, J. H. A. (1993) *Biochemistry 32*, 9772−9780.
38. Szalai, V. A., and Brudvig, G. W. (1996) *Biochemistry 35*, 1946−1953.
39. Tang, X.-S., Randall, D. W., Force, D. A., Diner, B. A., and Britt, R. D. (1996) *J. Am. Chem. Soc. 118*, 7638−7639.
40. Peloquin, J. M., Campbell, K. A., and Britt, R. D. (1998) *J. Am. Chem. Soc. 120*, 6840−6841.
41. Dorlet, P., Di Valentin, M., Babcock, G. T., and McCracken, J. L. (1998) *J. Phys. Chem. B 102*, 8239−8247.
42. Lakshmi, K. V., Eaton, S. S., Eaton, G. R., Frank, H. A., and Brudvig, G. W. (1998) *J. Phys. Chem. B 102*, 8327−8335.

43. Dorlet, P., Boussac, A., Rutherford, A. W., and Un, S. (1999) *J. Phys. Chem. B 103*, 10945−10954.
44. Matsukawa, T., Mino, H., Yoneda, D., Kawamori, A. (1999) *Biochemistry 38*, 4072−4077.
45. Berthold, D. A., Babcock, G. T., and Yocum, C. F. (1981) *FEBS Lett. 134*, 231−234.
46. Ford R. C., and Evans, M. C. W. (1983) *FEBS Lett. 160*, 159−164.
47. Styring, S., and Rutherford, A. W. (1988) *Biochim. Biophys. Acta 933*, 378−387.
48. Brudvig, G. W., Casey, J. L., and Sauer, K. (1983) *Biochim. Biophys. Acta 723*, 366−371.
49. Vass, I., and Inoue, Y. (1992) in *The Photosystems: Structure, Function and Molecular Biology* (Barber, J., Ed.) pp 259−294, Elsevier Science Publishers B.V., Amsterdam.
50. Lavergne, J., and Etienne, A. L. (1980) *Biochim. Biophys. Acta 593*, 136−148.
51. Sane, P. V., and Rutherford, A. W. (1986) in *Light emission by plants and bacteria* (Govindjee, Amesz, J., and Fork, D. C., Eds.) pp 329−360, Academic Press Inc., New York.
52. Demeter, S., Goussias, Ch., Bernat, G., Kovacs, L., and Petrouleas, V. (1993) *FEBS Lett. 336*, 352−356.
53. Kanazawa, A., Kramer, D., and Crofts, A. (1992) in *Research in Photosynthesis* (Murata, N., Ed.) Vol. II, pp 131−134, Kluwer Academic Publishers, Dordrecht, The Netherlands.
54. Rutherford, A. W., and Zimmermann, J. L. (1984) *Biochim. Biophys. Acta 767*, 168−175.
55. Nugent, J. H. A., Doetschman, D. C., and Maclachlan, D. J. (1992) *Biochemistry 31*, 2935−2941.
56. Boussac, A. (1997) *J. Biol. Inorg. Chem. 2*, 580−585.
57. Baxter, R., Krausz, E., Wydrzynski, T., and Pace, R. J. (1999) *J. Am. Chem. Soc. 121*, 9451−9452.

BI000131C